UDC 551.465

Sandeep Patil[1], Xian gui Li[2], Chi wai Li[1], Barry Y. F. Tam[1],
Cynthia Y. Song[1], Yong P. Chen[1], Qing he Zhang[3]

Longitudinal dispersion in wave-current-vegetation flow

The flow, turbulence and longitudinal dispersion in wave-current flow through submerged vegetation are experimentally examined. Laboratory experiments are carried out by superimposing progressive waves on a steady flow through simulated submerged vegetation. The resultant wave-current-vegetation interaction shows strong interfacial shear with increase in velocity due to wave-induced drift. The increase in turbulence in vegetation region is found to be about twice than in no wave case due to the additional mixing by wave motions. Solute experiments are conducted to quantify wave-current-vegetation longitudinal dispersion coefficient (WCVLDC) by routing method and by defining length and velocity scales for wave-current-vegetation flow, an empirical expression for WCVLDC has been proposed. Although increase in vertical diffusivity is observed compare to bare-bed channel, the shear effect is stronger which increases the magnitude of WCVLDC. The study can be a guideline to understand the combine hydrodynamics of wave, current and vegetation and to quantify the longitudinal dispersion therein.

1. Introduction. The understanding of transport and mixing processes like advection and diffusion is important to verify the acceptable limit of pollutants that are released into open channel systems. Apart from these processes, short period surface waves often exist due to the ubiquity of wind shear and contribute in mixing of pollutants [1]. Another influential agent is the common vegetation growth on the channel bed which hydrodynamically enhances the turbulence and associated mixing processes [2 – 4]. The resultant flow is the combination of wave, steady current and vegetation which generally exists in nature. Knowledge of the combine hydrodynamics of wave-current-vegetation is practical in understanding the particulate sediment transport [5], exchange of vertical momentum transfer [6] and also distortion of plant morphology [7, 8]. In this paper, the flow, turbulence and longitudinal dispersion in this combine flow field of wave-current-vegetation is experimentally examined. The depth-wise velocity profiles and turbulence have been measured and by conducting dye studies, an empirical expression for the longitudinal dispersion coefficient for wave-current-vegetation flow (WCVLDC) is proposed. The results of this study will improve the understanding of the hydrodynamics and pollutant mixing in the combine wave-current-vegetation flow. The paper is organized as follows. Section 1 provides introduction followed by brief literature on wave-current and current-vegetation studies in Section 2. Experimental procedure is described in Section 3. Section 4 includes the results on velocity and solute concentration profiles with proposed expression for WCVLDC. Section 5 presents the conclusion of this study.

2. Review of literature. After the initial work on modeling vegetation as an increased bottom roughness [9, 10], recent studies focus on velocity profiles and turbulent characteristics of steady flow through vegetated channels [11, 12]. In

emergent vegetation, where $d < h_s$ (d is the flow depth; h_s is the vegetation stem height), the increase in the head loss increases the vegetative velocity compare to open channel [13, 14]. Also, the depth-wise vegetated velocity shows more uniformity because of the presence of stems that reduces the shear [15, 16]. Moreover, the turbulent eddies of stem-diameter scale increase the turbulence within vegetation [17] and cause increase in vertical diffusivity over to that in bare-bed flow. The reduced shear with increased vertical diffusivity act to reduce the longitudinal dispersion coefficient in the emergent vegetation. Moreover, solute transport studies in this flow shows trapping of solute in the stem-wake regions and causes «frontal delay» (Fig. 6, [14]) which is the difference between the observed concentration – time ($C - t$) curve and the corresponding theoretical curve by well-known 1-D dispersion equation.

In submerged vegetation $(d > h_s)$, an overflow region exists above the vegetation region with a strong shear layer at the interface between two regions due to the large difference of velocities between these regions [6, 18]. Moreover, [19] observed that the depth-wise hydrodynamics in vegetation region shows two parts, the vertical exchange zone (VEZ) in the upper part of h_s which is influenced by vertical intrusion of mass and momentum from overflowing water and the longitudinal exchange zone (LEZ) below VEZ till bottom in which hydrodynamics is similar to that of emergent vegetation described before. They showed that the relative depths of these zones depend on the height of overflow. The depth-wise velocity profile is uniform in LEZ and increases in VEZ with strong shear to join the higher overflow velocity above h_s (Fig. 1).

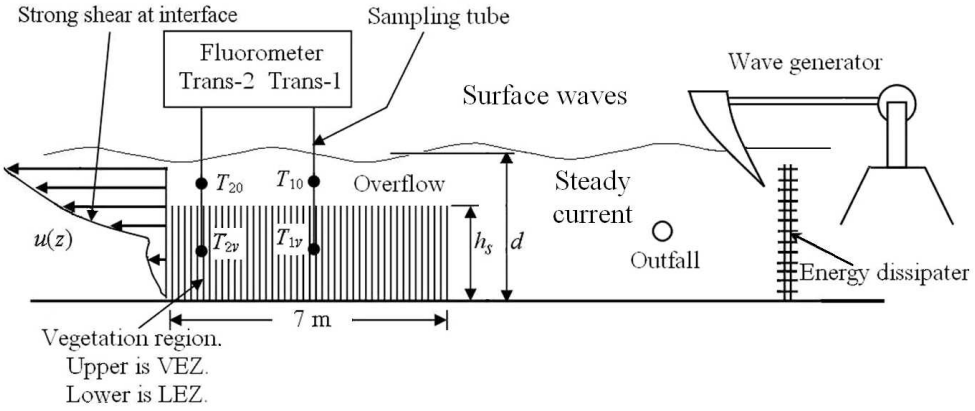

F i g. 1. Experimental set-up

This velocity distribution using Prandtl's mixing length approach was derived in [20] who also proposed a relation between velocity and turbulent intensity. The vertical turbulent diffusion has been observed to be higher around interface and lower in above and below it [19, 21]. The strong shear effect at the interface is expected to increase the longitudinal dispersion coefficient in submerged vegetation compare to that in emergent vegetation and bare-bed channel. The presence of surface waves in such flows will have additional wave-associated drift velocity [22]. In the wave-current flows without vegetation, this drift from the oscillatory part of the flow field

is the mass transport velocity that causes finite longitudinal dispersion [23 – 25]. The amount of wave-induced dispersion in bared bed flows depends on wave amplitude (a) and wave period (T) which is parameterized by [1] and [26]. The oscillatory movement of the particles also affects the mixing characteristics by inducing near bed shear [27]. A theoretical study on wave and current flow in vegetation [28] suggested that the drag coefficient of current-vegetation flow is too large to simulate the flow profile of wave-current-vegetation flow. They obtained $C_d = 0.6$ to simulate the profile in flexible vegetation. [29] have proposed a 2-layer model to predict the longitudinal dispersion in flow through submerged vegetation in absence of wave activity in which the dispersion coefficient has been quantified as an addition of the dispersion due to the three scales of mixing, *viz.* the smaller stem-scale mixing near the lower part of the canopy, the coherent KH vortices-scale mixing in the shear layer and the depth-scale mixing in the overflow region.

Thus, in general, it can be deduced that the longitudinal dispersion of steady flow will be affected by the presence of surface waves as well as vegetation. The resultant dispersion coefficient will be WCVLDC which is quantified in this paper. The laboratory experiments are conducted to measure the velocity profiles, turbulence and solute concentration at selected transects in absence/presence of waves are measured and described in the following Section.

3. Experimental set-up and procedure. Experiments are conducted in a 15 m long, 31 cm wide glass wall flume with smooth steel bottom. A steady recirculating uniform current is generated by passing the pumped flow through energy dissipaters as shown in Fig. 1. The energy dissipaters are followed by baffle walls to dampen the surface fluctuations to get a smooth horizontal surface. Bed slope $S_0 = 0.0001$ is kept constant and the flow discharge (Q) is varied to get different velocities. A wave maker is placed downstream of the baffle walls to generate progressive surface waves on this smooth uniform flow. The tailgate hinged at bottom at the rear end allows the waves to pass over it without reflecting back which avoids the need of a wave-absorbing beach. A vegetation model, 7 m long in flow direction is simulated using thermoplastic rubber rods that are glued in the holes drilled on an acrylic sheet. The height of the rubber rods (*i. e.* stem height) $h_s = 15$ cm is maintained. This stem height with the total flow depth $d = 25$ cm (overflow depth is 10 cm) represents a typical set up of confined submerged vegetation in which the surface waves, strong interfacial shear, VEZ and LEZ are active in the flow domain [19]. Two vegetation canopies of different densities are modeled by using rods of diameters, 6 mm and 8 mm. The constant centre to centre spacing between the rods, $\Delta S = 30$ mm is maintained in both the canopies to form a square grid. This provides vegetation density, $V_d = d_s^2 / \Delta S^2 = 0.04$, *i. e.* 4% for $d_s = 6$ mm and $V_d = 0.07$, *i. e.* 7.1% for $d_s = 8$ mm. After initial transition due to vegetation interference, flow attains steady state and maintains through out the remaining part of the vegetation. This steady state part of vegetation is selected to measure velocity, turbulence and solute concentration. The rods are placed wall to wall to prevent the streaming effect close to the wall. The secondary flow generated above the vegetation model can be neglected because of the overflow depth being small, the instantaneous turbulent intensity at interface is much larger than the RMS value [6].

3.1. ***Flow measurement.*** Depth-wise velocity profiles and turbulent intensities are measured in no-wave (current-vegetation) and with-wave (wave-current-vegetation) cases. Ultrasonic velocity profiler (UVP) with vertically arranged five transducers is employed at mid-width to measure the depth-wise velocity and turbulence profiles along flow direction. The vertical spacing between transducers is 50 mm with the lowest transducer is at a distance of 25 mm from the channel bed. Thus lower three transducers measured in-canopy velocities whereas the upper two measured overflow velocities. Wherever required, two or three rods are displaced to clear the optical path of the transducers from stem interference. Each transducer sampled the time series of the velocity profile at 50 Hz frequency at several points within 150 mm from its tip along the flow direction. For the current-vegetation cases, the instantaneous velocities are sampled for sufficient duration and are averaged over time and space to get the mean velocity. The turbulent intensity is measured by averaging the fluctuating signals of UVP over the mean velocity.

For wave-current-vegetation experiments, progressive waves are passed over the steady current to get wave-current-vegetation flow field. Waves with wave height and period between 1.5 cm & 4 cm and 1.5 s & 4 s respectively, are maintained to follow shallow wave and short period condition. The UVP signals for 250 – 300 wave oscillations are collected and averaged to get the Eulerian-mean velocity. For the turbulent intensity in with-wave flow, the instantaneous velocity (u_i) of UVP has three components, *viz.* the mean of instantaneous velocity $u(z)$, the time-dependent velocity, $\tilde{u}(z,t)$ and the fluctuation turbulent velocity $u'(z,t)$. The phase-averaged velocity $\langle u \rangle = \tilde{u} + u$, is average of samples taken at fixed phase in the imposed oscillations and is obtained as $\langle u \rangle = \frac{1}{N}\sum_{n=0}^{N} u_i(t+nT)$, where n is the oscillation cycle number and N is the total oscillation cycles. This $\langle u \rangle$ is subtracted from the UVP signals, u_i to get the turbulent intensity in wave-current-vegetation flow.

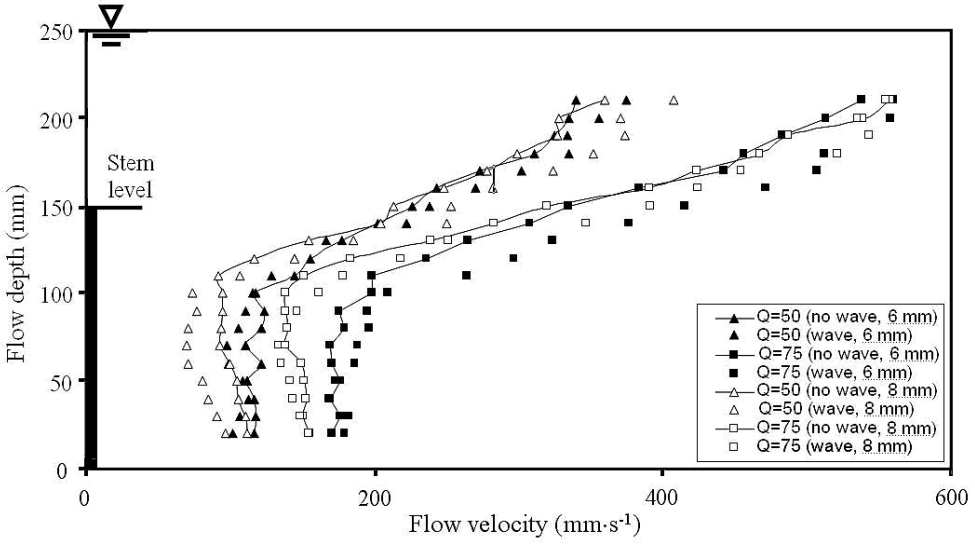

F i g. 2. Depth-wise velocity profiles in current-vegetation and wave-current-vegetation flows

The measurement is repeated for Q = 50 $m^3 \cdot h^{-1}$, 75 $m^3 \cdot h^{-1}$ & 90 $m^3 \cdot h^{-1}$ in no-wave and with-wave cases. Fig. 2 and 3 show the measured velocity profiles and turbulent intensity in case of Q = 50 $m^3 \cdot h^{-1}$ and 75 $m^3 \cdot h^{-1}$ for both $V_d = 4\%$ and 7%, respectively. Looking at the high distortion of velocity and turbulence in Q = 75 $m^3 \cdot h^{-1}$, the case of Q = 90 $m^3 \cdot h^{-1}$ is not plotted. For all the experiments described above, the surface slope (S_f) over vegetation region is measured using a pair of water level gages, each located little outside the either ends of vegetation model. Because $S_f >> S_0$ in presence of vegetation, S_f governs the flow and therefore used in place of S_0 in vegetation experiments, whereas S_0 is maintained in the experiments in bare-bed channel.

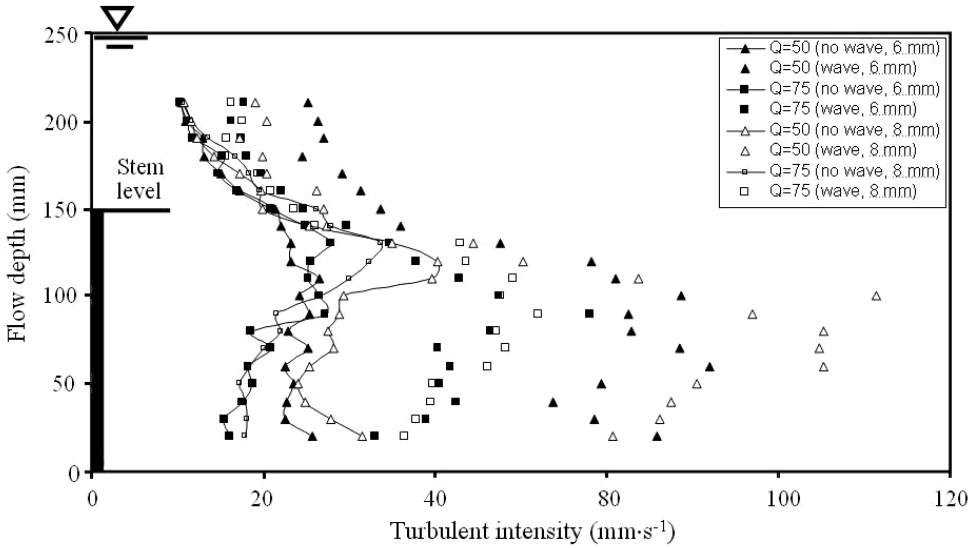

F i g. 3. Depth-wise turbulent intensities in current-vegetation and wave-current-vegetation flows

3.2. ***Solute measurement.*** A 20% active solution of rhodamine dye is injected from a constant head tank in the wave-current-vegetation flow described above, through a solute outfall. The outfall is a 5 mm diameter acrylic tube placed width-wise to form a line source of solute. The tube has 0.5 mm diameter holes in four lines facing the flow direction. The outfall is placed well before the vegetation so that solute should achieve cross-sectional uniformity before entering the vegetation region. Some distance after entering the vegetation, surface waves owing to their large scale depth-wise orbital motions, cause solute to spread uniformly across the cross section of flow. Solute concentration is measured in overflow as well as vegetation region and concentration verses time ($C - t$) curves have been plotted for both the regions. The uniformity is experimentally determined where the difference in the concentration in vegetation and overflow region becomes less than 5%. The length of canopy after this cross-sectional uniformity is used to locate sampling transects. Two transects (T_1 and T_2 in Fig. 1) are located to apply routing procedure [30] to calculate dispersion coefficient. At both the transects, the solute concentration at mid-depth of overflow (T_{10} and T_{20}) and mid-depth of vegetation (T_{1v} and T_{2v}) is measured continuously along time, using 10-AU fluorometer and

recorded through data acquisition system. The sampling points are shown in black dots. Two black dots on each sampling tube are the sampling points on each transect. Upper dots sample from the mid-depth mid-width of overflow region (T_{10} and T_{20}). Lower dots sample from the mid-depth mid-width of vegetation region (T_{1v} and T_{2v}). Thus, there are two transects (T_1 and T_2) and at each transect, the solute concentration is measured at two sampling points, *i. e.* solute is sampled at four locations (T_{10}, T_{1v}, T_{20}, T_{2v}) as shown in Fig. 1.

The two concentration – time breakthrough curves ($C - t$ curves) from the two sampling points at each transect are used to find the difference of 5% stated above. The time for solute to reach to fluorometer from channel is estimated to be two seconds and accordingly, the $C - t$ curves are shifted. The dispersion in the small diameter sampling tube is assumed negligible. The contribution from the stem scale diffusion is negligible [14] and hence neglected. The dye study is repeated for five values of Q, *i. e.* 50 $m^3 \cdot h^{-1}$, 65 $m^3 \cdot h^{-1}$, 75 $m^3 \cdot h^{-1}$, 82 $m^3 \cdot h^{-1}$ and 90 $m^3 \cdot h^{-1}$.

In absence of waves, wave-induced oscillations are absent and the 2-point sampling at each transect provides the magnitude of the delay in solute transport through vegetation over that in overflow. This delay in percentage form is measured for various flow velocities. As the concentration measurement in vegetated region at transect-2 (*i. e.* T_{2v}) is required only to measure percentage delay over overflow, the concentration in vegetation at transect-1 (*i. e.* T_{1v}) is not measured in absence of waves.

3.3. ***Estimation of observed WCVLDC.*** The solute concentration measured at both transects is averaged over intervals of the wave period to get the period averaged steady values of concentration. The $C - t$ curves measured at transect-2 from the overflow (T_{20}) and from the vegetation region (T_{2v}) are indistinguishable due to the wave-induced mixing as seen in Fig.4.

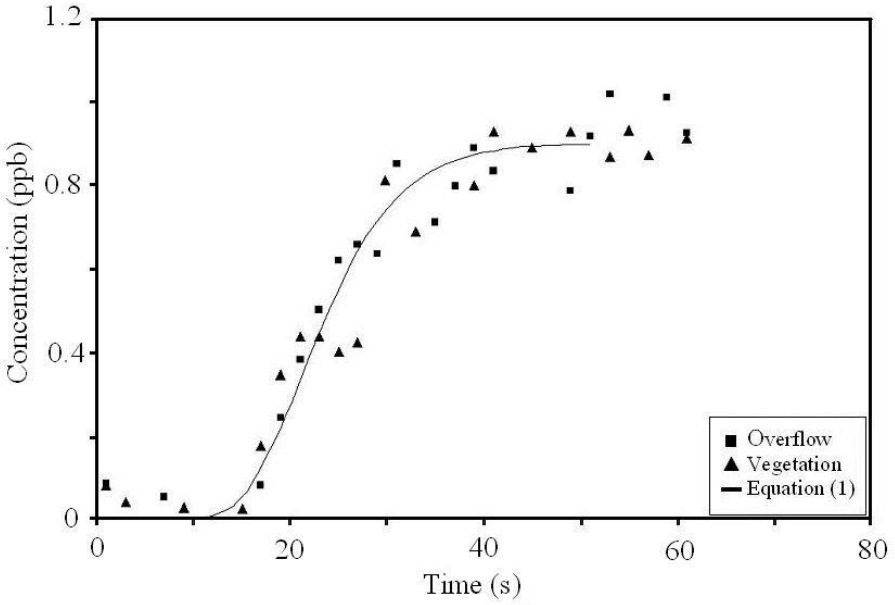

F i g. 4. $C - t$ curves in wave-current-vegetation flow for Q = 75 $m^3 \cdot h^{-1}$ and V_d = 4% (wave height is 3.5 cm, T = 2.3 s, E_{wvx} = 0.043 $m^2 \cdot s^{-1}$): measured in overflow region (▲), measured in vegetation region (■), theoretical profile by routing method (—)

The same merging between T_{10} and T_{1v} is observed at transect-1. Because of this merging, the $C - t$ curves at either T_{10} or T_{1v} and T_2 or T_{2v} are used in the routing method [30] to find WCVLDC. As the measured concentrations are period-averaged, the 1-D dispersion equation is also averaged over a wave period to get the period-averaged 1-D dispersion equation. The derivation is included in Appendix. Following frozen cloud assumption and superposition integral [31], the solution of equation (A6) is

$$\overline{C_{2p}}(t) = \int_0^\infty \overline{C_1}(t) \frac{\overline{U}}{\sqrt{4\pi E_{wvx}(t-\tau)}} \exp\left[\frac{(L-\overline{U}(t-\tau))^2}{4E_{wvx}(t-\tau)}\right] d\tau, \qquad (1)$$

where overbar denotes period-averaged steady value, $\overline{C_{2p}}$ is the predicted concentration at second transect which can be estimated from the observed concentration $\overline{C_1}$ at the first transect, L is the distance between the two transects, E_{wvx} is the WCVLDC and $\overline{U}$ is the depth-wise mean velocity in wave-current-vegetation flow. It is calculated from the velocity profiles measured in wave-current-vegetation flow (for example, see Fig. 2). The observed concentration at transect-1 (at either T_{10} or T_{1v}) is the $\overline{C_1}$ substituted in equation (1) and theoretical $C - t$ curve ($\overline{C_{2p}}$) for transect-2 is predicted (line graph in Fig. 4). This predicted data is superimposed over the measured data at transect-2 (at either T_{20} or T_{2v}) and the optimum value of WCVLDC is evaluated by least square method for five different discharges (Q = 50 $m^3 \cdot h^{-1}$, 65 $m^3 \cdot h^{-1}$, 75 $m^3 \cdot h^{-1}$, 82 $m^3 \cdot h^{-1}$ and 90 $m^3 \cdot h^{-1}$) and are used to work out an expression for WCVLDC in Section 4.2. The estimated uncertainty is calculated using IS code and found to be around 15%. The observed WCVLDC shows increasing trend with increase in current owing to the increase in the flow velocity that causes increase in interfacial shear and at the same time, increase in vegetative velocity which in turn reduces the turbulence and therefore diffusivity in vegetation. It is discussed in the following section.

4. Results

4.1. ***Flow velocity and turbulent intensity (in absence and presence of waves).*** In the current-vegetation flows, the mean velocity and turbulence intensity for V_d = 4% (d_s = 6 mm) and 7.1% (d_s = 8 mm) can be seen in Fig. 2 and 3 for Q = 50 $m^3 \cdot h^{-1}$ and 75 $m^3 \cdot h^{-1}$. [14] observed that in emergent vegetation, the increase in V_d reduces the bottom boundary layer thickness upto 50% which reduces the velocity shear in vegetation. The vertical velocity profiles in LEZ in Fig. 2 show the same phenomenon in present experiments because LEZ replicates emergent condition. However, the constant velocity in LEZ increases along depth in VEZ to adjust with the nearing higher velocity in overflow and displays strong shear which becomes stronger with increasing V_d (Fig. 2).

Comparison between vegetation densities shows that increase in V_d from 4% to 7% reduces the velocity in LEZ due to the corresponding increase in turbulence (Fig. 3) which is maximum at the interface [21]. This is in contrast to the emergent-vegetation case in which the mean velocity increases with V_d owing to the absence

of overflow region [14]. For higher Q = 75 $m^3 \cdot h^{-1}$, the reduction in vegetation velocity is compensated by increase in overflow velocity.

On the other hand, comparison between flow discharges for a fix V_d shows overall increase in velocity from 50 $m^3 \cdot s^{-1}$ to 75 $m^3 \cdot s^{-1}$, in turn decrease in turbulent intensities. It is noticed in Fig. 3 that in vegetation region, turbulent intensity of Q = 75 $m^3 \cdot h^{-1}$ in V_d = 4% is close to its value of Q = 50 $m^3 \cdot h^{-1}$ in V_d = 7.1%. This suggests that the increase in drag due to higher V_d can be achieved in lower V_d by increasing the flow velocity.

For the wave-current-vegetation flow, the same figures (Fig. 2 and Fig. 3) show period-averaged velocities and turbulent intensities, respectively (dots only data). All the trends described above have been observed to be followed in the presence of waves. In addition, increase in the velocity in overflow region is attributed to the additional wave-induced drift velocity [22]. Higher amplitude or lower wave period generates higher drift. The turbulent intensities in Fig. 3 clearly show higher level of turbulence in presence of wave especially in vegetated region because of the additional bidirectional motions of waves [32]. The bidirectional motions increase the interaction between near-wake and far-wake regions which can enhance the stem-scale turbulent eddies to the probable scale of ΔS and justify the increase in turbulence in wave-current-vegetation flow. Nonetheless, increase in Q in presence of waves shows decrease in in-canopy turbulence owing to the vegetation streaming.

Within a wave period, the flow structure is depending on the relative amplitude of wave-induced velocity and current. For higher wave amplitudes, the wave-induced speed being higher than current speed. Therefore, the instantaneous velocities of combine wave-current flow sometimes reverse in direction under wave trough. In such cases, wave-induced turbulence occurs at the front and back side of stems alternatively. Soon after the flow reverses, a temporary wake and recirculation region forms upstream of a stem with a temporary drag from behind. In solute studies, this periodic motion of water particles may reduce the trapping of solute in the wake region. On the other hand, if the waves are small in amplitude, then the net wave-current velocity within a wave period is always positive. In this case, stems experience a reduction in drag under wave trough due to the reduction in net wave-current velocity. The wave structure still remains unsteady and reduces the degree of trapping of solute in the wake region. Thus in the presence of waves (*i. e.* wave-current-vegetation flow), the turbulence and therefore the exchange of solute between near-wake region and far region enhances.

4.2. ***Empirical expression for WCVLDC.*** The WCVLDC estimated by routing method are used to derive an empirical expression for WCVLDC. First of all, this functional relationship of longitudinal dispersion coefficient is worked out using Elder's longitudinal dispersion coefficient [33] which is written as

$$E_x = -\frac{1}{d}\int_0^d u' \int_0^z \frac{1}{D_{z'}} \int_0^{z'} u' dz'' dz' dz \,, \tag{2}$$

where D_z is the vertical diffusivity; $u'(x, y, z, t) = u(x, y, z, t) - U$ is the local velocity fluctuations from the mean flow velocity, U. The term u' makes equation (2)

complicated to solve. Therefore, a mixing length analogous to Prandtl-mixing length is assumed to represent the fluctuating velocity, u' in equation (2), then u' can be simplified as

$$u' = l_d \frac{\partial u}{\partial z}, \tag{3}$$

where l_d is a vertical length scale to be determined and is not the Prandtl-mixing length. The direction of l_d is vertical because the shear velocity u, in Eq. 2 is in vertical direction. Substitution of equation (3) in equation (2), equation (2) is written as

$$E_x = -\frac{1}{d}\int_0^d \left(l_d \frac{\partial u}{\partial z} \right) \int_0^z \frac{1}{D_{z'}} \int_0^{z'} \left(l_d \frac{\partial u}{\partial z''} \right) dz'' dz' dz = f(l_d, u), \tag{4}$$

where D_z is also a function of l_d and u. It is obvious that $l_d = d$ for bare-bed channel. On the same line, for the transverse variation of shear, the well-known dispersion coefficient due to [31] (similar to equation (2)) shall provide $E_x = f(l_w, u)$, where l_w is some transverse length scale which, for bare-bed channel is the width of the channel, W. Based on these scales, Eq. 4 in the form of functional relationship can be written as

$$E_x = f(l_w, l_d, u). \tag{5}$$

Equation (5) shows that the accuracy of dispersion coefficient is to find the correct expressions for the distance and velocity scales. Several expressions of longitudinal dispersion coefficients for bare-bed channel proposed in the past have been based on equation (5). These scales are modified to include the effect of vegetation and waves and then used to work out a simple empirical expression for WCVLDC.

First of all, the longitudinal dispersion coefficient for the bare-bed channel is estimated by usual dye experiments. These observed values along with the observed data of [14] for bare-bed channel, are found to be matching with the empirical expression of dispersion coefficients given by [34] as

$$\frac{E_x}{qS_0} = 0.253 \left(\frac{W}{R} \right)^{2.11} \left(\frac{U}{U_*} \right)^{-1.06} {S_0}^{-0.98}, \tag{6}$$

where E_x is the longitudinal dispersion coefficient in bare-bed channel, qS_0 is the fluid power (q is discharge per unit width), W/R is the aspect ratio, W is the channel width and $R = Wd/(W+2d)$ is the hydraulic radius, U/U_* is the friction factor and $U_* = \sqrt{gRS_0}$ is the shear velocity. For the present experiments, $W/R = 0.31/0.095 = 3.24$. For this ratio, secondary currents appear in lower magnitude of velocities due to which equation (6) overestimates the dispersion coefficients (see point P in Fig. 5). Also equation (6) is based on laboratory as well as field data and thus it includes field specific conditions such as heterogeneity in bed, river meandering, non-prismatic cross section and tends to increase the dispersion coefficient. For the higher magnitude of velocities, secondary currents are negligi-

ble for which the dispersion coefficient is nearing the observed value which in turn shows reduced effect of secondary currents. Similarly, the data of [14] is reasonably close to the predictions of equation (6) because it is measured in wider flume (for which $R = d$ in equation (6)) which eliminates secondary current effects.

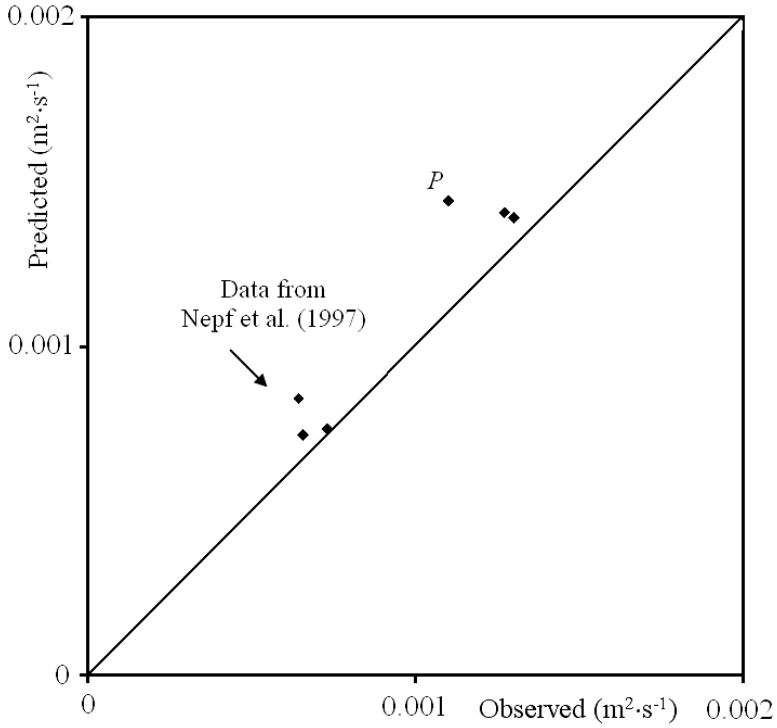

F i g. 5. Observed and predicted by equation (6) longitudinal dispersion coefficient ($m^2 \cdot s^{-1}$) in bare-bed channel

Thus Eq. 6 is acceptable except in case of lower magnitude of velocities in bare-bed condition. This limitation does not exist in presence of vegetation where pure water depth (overflow depth) reduces from 25 cm to 10 cm and for which $W/R = 5.1$ is closer to shallow water flow. Therefore, equation (6) is considered and extended for the effect of vegetation and waves. To include these effects, the functional relationship of equation (6) is assessed and written as

$$\frac{E_x}{qS_0} = f\left(\frac{U}{U_*}, \frac{W}{d}\right) = f(W, d, U) \ , \tag{7}$$

where U_* and q are function of W, d and U. Comparison of equation (7) with equation (5) shows $l_d = d$, $l_w = W$ and $u = U$. These scales are to be modified to include the effect of waves and vegetation in equation (6). For the effect of wave, a dimensionless wave parameter a/TU_* [26] is used where a is the wave amplitude and T is the wave period. The effect of vegetation is included by modifying the transverse and vertical length scales and the velocity scale in equation (6) as follows.

Transverse length scale (l_w). The extremities of vegetation density are considered, non-vegetation and very dense vegetation, *i. e.* complete blockage of flow through vegetation region. For non-vegetation case (d_s = 0), l_w should be *W*. For full vegetation-blockage (d_s = ΔS), the transverse scale should still be *W* as full channel width is still exist in overflow region for the water to flow. Based on these limiting conditions, dimensionless vegetation density $a_s d_s$ is used as vegetation parameter and an expression for l_w is formulated as

$$l_w = W - \left[d_s\left(1 - a_s d_s\right)\right]^{\Omega_1}. \tag{8}$$

Equation (8) can be tested for the two extremities. Thus, for non-vegetation case, d_s = 0 and equation (8) provides, $l_w = W$. For the full vegetation-blockage, $a_s d_s$=1 and for which again $l_w = W$. Parameter Ω is used to represent the trend of equation (8) between these extremities. As only two vegetation densities are studied in this paper, linear relationship of equation (8) is assumed by assigning $\Omega_1 = 1$.

Vertical length scale l_v. The two extremities explained above are applied to find l_v. For no-vegetation case, l_v should be *d*. For the complete blockage of vegetation region $V_d = 1$, l_v should be the depth of overflow region, *i. e.* $d - h_s$. Based on these values, l_v is formulated as

$$l_v = d - h_s\left(a_s d_s\right)^{\Omega_2} = d - h_s\left(\frac{d_s^{\,2}}{\Delta S^2}\right)^{\Omega_2}. \tag{9}$$

It can be verified that, for no-vegetation case (d_s = 0), equation (9) provides $l_v = d$ whereas for full vegetation-blockage case ($d_s = \Delta S$), equation (9) becomes $l_v = d - h_s$. Linear relationship of equation (9) is assumed by assigning $\Omega_2 = 1$.

Velocity scale (*denoted as U_v*). The flow discharge *Q* is a known quantity and is kept constant in absence or presence of vegetation by maintaining constant rate of pumping. For the bare-bed channel, velocity scale is $U = Q/Wd$ whereas in presence of vegetation, $U_v = Q/l_w l_v$. Thus, using equations (8) and (9), U_v can be written as

$$U_v = \frac{Q}{l_w l_v} = \frac{Q}{\left\{W - \left[d_s\left(1 - a_s d_s\right)\right]\right\}\left[d - h_s\left(a_s d_s\right)\right]}. \tag{10}$$

It can be seen that U_v eventually depends on vegetation density and vegetation height. In the absence of vegetation (d_s = 0), U_v reduces to *U* satisfying the required condition for bare-bed channel. For the full blockage condition, equation (10) provides $U_v = Q/[W\left(d - h_s\right)]$, *i. e.* discharge through overflow region.

The above defined vegetative scales are replaced in equation (6), *i. e.* $W = l_w$, $d = l_v$ and $U = U_v$ to include effect of vegetation. The S_0 is replaced by S_f and shear velocity $U_* = \sqrt{g l_v S_f}$ where g = 9.81 m·s^{-2}. Also wave parameter as mentioned before is included for the effect of wave. Thus, equation (6) becomes

$$\frac{E_{wvx}}{qS_0} = \alpha \left(\frac{l_w}{l_v} \right)^{\beta} \left(\frac{U_v}{U_*} \right)^{\gamma} S_0^{\zeta} \left(1 + \phi_1 \frac{a}{TU_v} \right)^{\phi_2} , \qquad (11)$$

where $\alpha = 0.258, \beta = 2.062, \gamma = -1.121, \zeta = -0.956$, ϕ_1=17.08 and ϕ_2 = 3.31 are the regression coefficients (correlation coefficient is 0.96) computed by least square method. The magnitude of ϕ_1 ~ 17 suggests that the magnitude of wave parameter should be higher by an order and thus keeps further scope for trying different combinations of wave parameter. Nonetheless, the proposed WCVLDC (see equation (11)) provides first hand information in view of no work on the pollutant dispersion in combine wave-current-vegetation flow field. The observed values of WCVLDC from Section 3.3 are used to obtain equation (11). The observed [equation (1)] and predicted WCVLDC are shown in Fig. 6. For the bare-bed channel, a and d_s are zero and equation (11) reduces close to equation (6). Equation (11) is based on limited data due to the laboratory constraints. However, it can serve as a preliminary guideline for assessment of dispersion in wave-current-vegetation interaction.

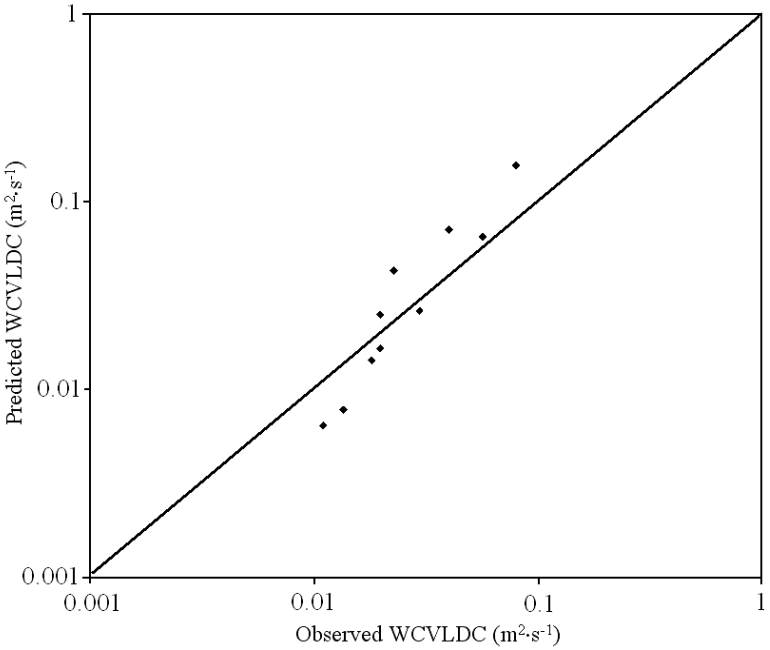

F i g. 6. Observed and predicted WCVLDC (equation (11))

In absence of wave activity, the $C - t$ curves in vegetation and overflow regions separate and become distinct (Fig. 7). The separation is caused by the delay in vertical mixing of solute between the two regions because of the absence of wave-induced oscillations. The delay in percentage form is measured at the ends of the $C - t$ curves. The interfacial strong shear causes Kelvin – Helmholtz coherent vortices at the interface [35] that are thought to restrict rather than support the downward spreading of solute across the interface [29]. Because of the delay, the necessary condition of cross-sectional uniformity of solute could not be achieved and hence equation (11) is not valid in absence of waves.

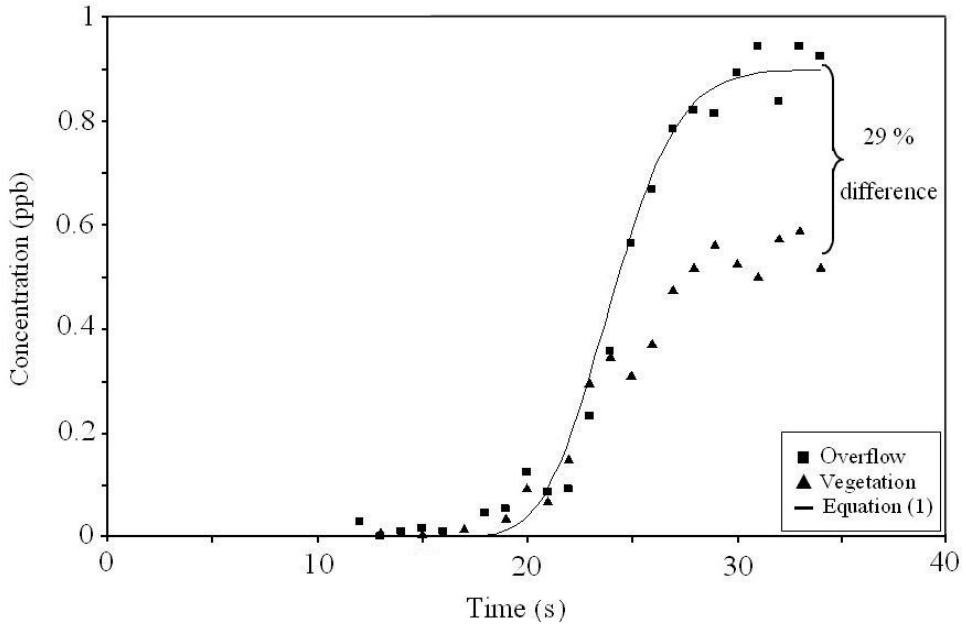

F i g. 7. *C – t* curves in current-vegetation flow for Q = 75 $m^3 \cdot h^{-1}$ showing % solute delay in vegetation: measured in overflow region (▲), measured in vegetative region (■), theoretical profile by routing method (—)

However, in practical situation like in coastal fields, a combine hydrodynamics of wave – current – vegetation exists in which because of the surface waves, the pollutants are always vertically well mixed. Motivating from this, wave activity is used in this laboratory study to get uniform spreading of solute across the combine cross section of vegetation and overflow region. Effect of increase in wave amplitude on WCVLDC can be studied as a further extension to this study. Increase in wave amplitude may increase WCVLDC because of increase in drift velocity [22] that causes additional shear [25] and also because the scale of wave-induced enhanced eddies in vegetation is limited by ΔS, increase in wave amplitude could not increase turbulence and therefore diffusivity beyond a certain limit. Experiments can be extended to verify this possibility.

4.3. ***Vertical diffusivity in wave-current-vegetation flow.*** The vertical diffusivity in wave-current-vegetation flow is difficult to measure experimentally. Therefore it is estimated by back calculation of Eq. 2 of Elder's dispersion coefficient [33]. Equation (2) is averaged over a wave period to get wave-current longitudinal dispersion coefficient (E_{wx}) as

$$E_{wx} = -\frac{1}{d}\int_0^d \overline{u' \int_0^z \frac{1}{D_{z'}} \int_0^{z'} u' dz'' dz' dz} \ , \qquad (12)$$

where overbar represents the period-averaged quantities. Assuming constant diffusivity, the wave-current shear term, $\bar{I}$ can be separately calculated ($\bar{I} = E_{wx} D_z$). If the period-averaged velocity and the solute data from Fig. 2 and Fig. 4 measured in

wave-current-vegetation flow is used, then equation (12) provides WCVLDC (E_{wvx}) and can be written as

$$E_{wvx} = -\frac{1}{d}\int_0^d \overline{u'\int_0^z \frac{1}{D_{z'}}\int_0^{z'} u'dz''dz'dz} = \frac{I_{wcv}}{D_{zwcv}}, \qquad (13)$$

where I_{wcv} and $D_{zwcv} = D_z$ = const are the wave-current-vegetation induced shear and the vertical diffusivity, respectively. The observed WCVLDC estimated by routing method in Section 3.3 are substituted in E_{wvx} of equation (13). I_{wcv} is estimated from the depth-wise measured velocities in wave-current-vegetation flow and using equation (13), the magnitude of D_{zwcv} is calculated. For example, for Q = 50 $m^3 \cdot h^{-1}$ and wave of height ~ 2 cm and period ~ 1.5 s, observed WCVLDC = = 78 $cm^2 \cdot s^{-1}$ is estimated from the routing procedure. The $I_{wcv} \sim 8800$ $cm^4 \cdot s^{-2}$ is calculated from the corresponding depth-wise velocity profile provides $D_{zwcv} \sim 113$ $cm^2 \cdot s^{-1}$ which is about two order higher than the value in bare-bed channel ($D_z \approx 0.067 U_* d \sim 3.2\,cm^2 \cdot s^{-1}$, U_* is shear velocity [36]). Table shows E_{wvx}, I_{wcv} and corresponding D_{zwcv} in Q = 50 $m^3 \cdot h^{-1}$ for both the stem densities. The increase in the vertical diffusivity over that in bare-bed channel is attributed to increased turbulence in presence of stem-scale vegetation and wave-induced enhanced eddies. Table also shows dispersion coefficient in bare-bed channel that are lower in magnitude than WCVLDC which suggests higher influence of interfacial shear on WCVLDC than vertical diffusivity.

Vertical diffusivity, shear and WCVLDC for Q = 50 $m^3 \cdot h^{-1}$, V_d = 4% and 7%

Value	Bare-bed (no wave)	Stem density (%)	
		4.0	7.1
D_{zwcv} ($cm^2 \cdot s^{-1}$)	3.15	112.5	150.0
I_{wcv} ($cm^4 \cdot s^{-2}$)	8.64	8794.0	9720.0
E_{wvx} ($cm^2 \cdot s^{-1}$) (observed)	14.40	78.2	64.8
E_{wvx} ($cm^2 \cdot s^{-1}$) (predicted)	11.00	102.0	55.0

5. Conclusions. This study presents characteristics of flow, turbulence and longitudinal dispersion in submerged vegetation under waves and current. As the combine wave-current-vegetation flow field is common in real wetland flows, the results of this study may be useful in context of studying exchange of CO_2, dissolved nutrients, sediment dynamics in submerged vegetation. Presence of waves increases the magnitude of steady current in overflow, improves the exchange between overflow and vegetation regions and also induces enhanced-scaled turbulence in vegetation that is favorable to biological transport like larvae [37] or pollen dispersion [38]. The resultant turbulence intensity is observed to be around twice the intensity in non-wave flows. The wave-induced increased turbulence and exchange between the two regions help releasing pollutants trapped within stem wakes which results in cross-sectional uniform distribution of pollutants, a neces-

sary condition to assess dispersion coefficient. The resultant WCVLDC estimated from dye experiments shows increasing trend with increase in the wave-current velocity. This is attributed to the contradictory trend of increasing interfacial shear and decreasing turbulence under increasing flow velocity. If compared with bare-bed channel, the shear effect in wave-current-vegetation flow is stronger. Therefore, although vertical diffusivity increases in presence of wave and vegetation, WCVLDC is always higher than that in bare-bed channel. In absence of wave, trapped pollutants in stem wakes could not be released in the flow direction and together with reduction in the vertical exchange between vegetation and overflow, results in delayed vertical transport of pollutants. Thus, due to the lack of cross sectional uniformity of solute, dispersion coefficient could not be assessed in the present design of experimental set-up. The outcome of this study, though based on limited experiments due to laboratory constraints, can serve as a guideline for the possible applications and advances in wetland mechanics where wave-current flow through vegetation is ubiquitous.

Acknowledgement This work was supported by a grant from the Research Grant Council of the Hong Kong Special Administrative Region (Project No 5048/99E, GT-649) and a grant from Beijing IS & T University (NSFC10671023).

Appendix

Wave-period-averaged 1-D dispersion equation for submerged vegetation

The one-dimensional dispersion equation for a straight and prismatic channel is written as

$$\frac{\partial C}{\partial t}+\frac{\partial (U C)}{\partial x}=\frac{\partial}{\partial x}\left(E_x \frac{\partial C}{\partial x}\right), \tag{A1}$$

where x, t, U, C, and E_x are the longitudinal distance, time, cross-sectional averaged longitudinal flow velocity, cross-sectional averaged concentration and longitudinal dispersion coefficient respectively. In the presence of linear periodic surface waves, equation (A1) is averaged over one-wave period as

$$\frac{\partial \overline{C}}{\partial t}+\overline{U\frac{\partial C}{\partial x}}=\overline{\frac{\partial}{\partial x}\left(E_x \frac{\partial C}{\partial x}\right)}, \tag{A2}$$

where overbar denotes the period-averaged value. The product term $\overline{U\cdot \partial C/\partial x}$ can be decomposed into the following forms by applying the Reynolds averaging procedure as

$$\overline{U\frac{\partial C}{\partial x}}=\overline{(\overline{U}+u')\frac{\partial(\overline{C}+c')}{\partial x}}, \tag{A3}$$

where $u'(t)$ and $c'(t)$ are respectively the temporal deviation of the velocity and the concentration from the corresponding period-averaged values. If steady current and progressive waves coexist in the channel, u' may be the wave velocity which is sinusoidal. The frozen cloud assumption can be used when the dynamic steady state of

the concentration distribution is attained. The concentration cloud will be advected back and forth by the sinusoidal velocity. The function $C(x_0, t)$, also $c'(x_0,t)$ and $\partial c'/\partial x\big|_{x_0,t}$, will be periodic and 90° out of phase with the sinusoidal velocity. Under this condition $\overline{u'C} \sim 0$, $\overline{u'c'}$, $\overline{u'\partial c'/\partial x} \sim 0$. Equation (A3) can be simplified to

$$\overline{U\frac{\partial C}{\partial x}} = \overline{U}\,\overline{\frac{\partial C}{\partial x}}. \tag{A4}$$

Similarly, the dispersion term can be written as,

$$\overline{\frac{\partial}{\partial x}\left(E_x\frac{\partial C}{\partial x}\right)} = \frac{\partial}{\partial x}\left(\overline{(\overline{E_x}+E_x')\frac{\partial(\overline{C}+c')}{\partial x}}\right) = \frac{\partial}{\partial x}\left(\overline{E_x}\frac{\partial\overline{C}}{\partial x} + \overline{E_x'\frac{\partial c'}{\partial x}}\right), \tag{A5}$$

where $E_x'(t)$ is the temporal deviation of the dispersion coefficient from the period-averaged dispersion coefficient. Since $E_x \sim U^2/\varepsilon$, where ε is the turbulent diffusion coefficient, E_x will be a periodic function of period T and is in phase with U. Consequently $\overline{E_x'\frac{\partial c'}{\partial x}}$ is expected to be very small in magnitude. The wave-period-averaged mass conservation equation can then be written as

$$\frac{\partial\overline{C}}{\partial t} + \overline{U}\frac{\partial\overline{C}}{\partial x} = \frac{\partial}{\partial x}\left(E_{wx}\frac{\partial\overline{C}}{\partial x}\right), \tag{A6}$$

where $E_{wx} = \overline{E_x}$ is the wave-current longitudinal dispersion coefficient and in the presence of vegetation, it is E_{wvx}, *i. e.* the wave-current-vegetation longitudinal dispersion coefficient.

REFERENCES

1. *Zeidler R. B.* Coastal dispersion of pollutants // J. Waterways, Harbours Coastal Eng. Div. ASCE. – 1976. – 102. – P. 235 – 254.
2. *Kadlec R.* Overview: surface flow constructed wetlands // Water Sci. Technol. – 1995. – 32, № 3. – P. 1 – 12.
3. *Leonard L., Luther M.* Flow hydrodynamics in tidal marsh canopies // Limnology and Oceanography. – 1995. – 40. – P. 1474 – 1484.
4. *Dunn C., Lopez F., Garcia M.* Mean flow and turbulence in a laboratory channel with simulated vegetation // Civil Engineering Studies, Hydraulic Engineering Series. – 1996. – № 51. – 148 p.
5. *Gambi M. C., Nowell A. R. M., Jumars P. A.* Flume observations on flow dynamics // Zostera marina L. (Eelglass) Beds. Mar. Eco. Progress Series. – 1990. – 61. – P. 159 – 169.
6. *Ikeda S., Kanazawa M.* Three-dimensional organized vortices above flexible water plants // J. Hydraul. Eng. – 1996. – 122, № 11. – P. 634 – 640.
7. *Sand-Jensen K.* Drag and reconfiguration of freshwater macrophytes // Freshwater Biology. – 2003. – 48. – P. 271 – 283.
8. *Asaeda T., Fujino T., Manatunge J.* Morphological adaptations of emergent plants to water flow // Freshwater Biology. – 2005. – 50. – P. 1991 – 2001.

9. *Kouwen N., Unny T. E.* Flexible roughness in open channels // J. Hydraul. Div. ASCE. – 1973. – 99, № 5. – P. 713 – 728.
10. *Kadlec R.* Overland flow in wetlands: vegetation resistance // J. Hydraul. Eng. ASCE. – 1990. – 116. – P. 691 – 707.
11. *Klopstra D., Barneveld H. J., Van Noortwijk J. M., Van Velzen E. H.* Analytical model for hydraulic roughness of submerged vegetation // Proc. Theme A, 27th IAHR Congr. San Francisco. – 1997. – P. 775 – 780.
12. *Stone B.M., Shen H.T.* Hydraulic resistance of flow in channels with cylindrical roughness // J. Hydraul. Eng. – 2002. – 128, № 5. – P. 500 – 506.
13. *Kouwen N., Unny T.E., Hill H.M.* Flow resistance in vegetated channels // J. Irrig. Drain. Div. ASCE. – 1969. – 95, № 2. – P. 329 – 342.
14. *Nepf H., Mugnier C. G., Zavistoski R. A.* The effects of vegetation on longitudinal dispersion // Estuarine, Coastal and Shelf Sci. – 1997. – 44, № 6. – P. 675 – 684.
15. *Tsujimoto T., Kitamura T.* Velocity profile of flow in vegetated-bed channels // Progressive Report № 1. – Hyd. Lab., Kanazawa University, Japan. – 1990.
16. *Lopez F., Garcia M.* Open-channel flow through simulated vegetation: Suspended sediment transport modeling // Water Resources Res. – 1998. – 34, № 9. – P. 2341 – 2352.
17. *Nepf H. M.* Drag, turbulence and diffusion in flow through emergent vegetation // Water Resources Res. – 1999. – 35, № 2. – P. 479 – 489.
18. *Temple D. M.* Changes in vegetal flow resistance during long duration flows. Transaction of ASAE. – 1991. – 34, № 4. – P. 1769 – 1774.
19. *Nepf H., Vironi E. R.* Flow structure in depth-limited, vegetated flow // J. Geophys. Res. – 2000. – 105, № C12. – P. 28547 – 28557.
20. *Carollo F.G., Ferro V., Termini D.* Flow velocity measurements in vegetated channels // J. Hydraul. Eng. ASCE. – 2002. – 128, № 7. – P. 664 – 673.
21. *Shimizu Y., Tsujimoto T., Nakagawa H.* Numerical study on turbulent flow over rigid vegetation-covered bed in open channel // Proc. Japan Soc. of Civil Eng. – 1992. – 447, № II-19. – P. 35 – 44.
22. *Longuet-Higgins M. S.* Mass transport in water waves. Phil. Trans. Roy. Soc. Lond. A. – 1953. – 245. – P. 535-581.
23. *Dalrymple R. A.* Wave induced mass transport in water waves // J. Waterways, Harbour and Coastal Eng. Div. ASCE. – 1976. – 102, № 2. – P. 255 – 264.
24. *Pearson J. M., Guymer I., West J. R., Coates L. E.* Effect of wave height on cross-shore solute mixing // J. Waterway, Port, Coastal and Ocean Eng. ASCE. – 2002. – 128. – P. 10 – 20.
25. *Law A. W. K.* Taylor dispersion of contaminant due to surface waves // J. Hydraul. Res. – 2000. – 38. – P. 41 – 48.
26. *Patil S., Rastogi A. K., Zhang Q. H., Misra R., Ukarande S. K.* Shear flow dispersion in wave and current // China Ocean Eng. – 2007. – 21, № 4. – P. 549 – 560.
27. *Mei C. C., Jin K. R., Fan S. J.* Resuspension and transport of fine sediments by waves // J. Geophys. Res. – 1997. – 102, № C7. – P. 15807 – 15821.
28. *Ota T., Kobayashi N., Kirby J. T.* Wave and current interactions with vegetation // Proceedings of 29th Coastal Engineering Conference. – USA, ASCE. – 2004. – 1. – P. 508 – 520.
29. *Murphy E., Ghisalberti M., Nepf H. M.* Model and laboratory study of dispersion in flows with submerged vegetation // Water Resources Research. – 2007. – 43. – P. 1 – 12.
30. *Fischer B. H.* Dispersion predictions in natural streams // J. Sanitary Eng. Div. ASCE. – 1968. – 94, № 5. – P. 927 – 943.
31. *Fischer H.B., List J. E., Koh R. C. Y., Imberger J., Brooks, N. H.* Mixing in inland and coastal waters // San Diego, CA: Academic Press, 1979. – P. 50 – 54.
32. *Dean R., Dalrymple R.* Water wave mechanics for engineers and scientists. –Englewood Cliffs, New Jersey: Prentice-Hall Inc., 1991. – 353 p.
33. *Elder J. W.* The dispersion of marked fluid in turbulent shear flow // J. Fluid Mech. – 1959. – 5. – P. 544 – 560.

34. *Ahmed Z., Kothyari U. C., Ranga Raju K. G.* Longitudinal dispersion in open channel // J. Hydrau. Eng. ISH. – 1999. – 5, № 2. – P. 1 – 21.
35. *Patil S., Singh V. P., Rastogi A. K.* Monami wave through submerged vegetation // 6th Int. Symp. on Stratified Fluid. – Univ. of Western Australia, Perth, 11 – 14 December, 2006.
36. *French R. H.* Open-channel hydraulics. – New York: McGraw-Hill, 1985. – 705 p.
37. *Eckman J. E.* The role of hydrodynamics in recruitment, growth and survival of Argopecten irradians and Anomia simplex within eelgrass meadows // J. Exp. Marine Biol. Ecol. – 1987. – 106. – P. 165 – 191.
38. *Ackerman J. D.* Diffusivity in a marine macrophyte canopy: implications for submarine pollination and dispersal // American J. of Botany. – 2002. – 89, № 7. – P. 1119 – 1127.

[1]The Hong Kong Polytechnic University, Hong Kong
[2]Beijing IS & T University, China
[3]Tianjin University, China

Received June 7, 2007
Revised July 15, 2007

Экспериментально исследовано влияние растительности в жидкости на течение, интенсивность турбулентности и продольную дисперсию в системе волна – течение. В лабораторных экспериментах в установившемся течении создавались короткие волны, генерируемые волнопродуктором, и имитировалась подводная растительность (вегетация). Зона вегетации располагалась в придонной области и моделировалась системой вертикально подвешенных резиновых жгутов. Обнаружено возникновение больших сдвигов горизонтальной скорости течения в зоне перехода от области вегетации к чистой воде. Турбулентное перемешивание в зоне вегетации в два раза выше, чем в системе волна – течение без вегетации. Подводная растительность приводит к росту дисперсии движения вдоль канала. Увеличение скорости течения вызывает увеличение вертикальных сдвигов скорости и усиление продольной дисперсии. Вертикальное перемешивание с учетом вегетации на два порядка выше, чем при ее отсутствии. Выполнены серии экспериментов с целью количественной оценки влияния вегетации на дисперсию движения вдоль канала в зависимости от скорости течения, его глубины и концентрации подводной растительности. Предложены аппроксимации для экспериментально найденных зависимостей коэффициента продольной дисперсии от параметров задачи.